Strain-controlled bulge test

B. Erdem Alaca[a] and K. Bugra Toga
College of Engineering, Koc University, Rumeli Feneri Yolu 34450 Sariyer, Istanbul, Turkey
Orhan Akar and Tayfun Akin
Electrical and Electronics Engineering Department, Middle East Technical University, 06531 Ankara, Turkey

(Received 26 March 2008; accepted 4 August 2008)

A closed-loop approach is adopted to implement strain rate control during the bulge test. Due to the difficulty of measuring strains directly, the technique is based on the conversion of displacement measurements to the corresponding strains using the plane-strain formulation. The necessary temporal evolution of the midpoint displacement of a rectangular diaphragm is derived under the condition of constant strain rate and is imposed as a control criterion. The technique is demonstrated on 500-nm-thick Au diaphragms by applying strain rates ranging from 2×10^{-6} to 2×10^{-4} s^{-1}. By measuring the corresponding yield strength values, a strain rate sensitivity of 0.11 is obtained, which is close to what was previously reported on similar specimens using the microbending test.

I. INTRODUCTION

Bulge test is a versatile characterization method capable of determining a complete set of material properties of thin films under various thermodynamic conditions. It is based on measuring the deflection of a membrane under an applied pressure. The obtained pressure-deflection behavior is then utilized to extract a variety of properties using the membrane theory. Following the original work by Beams,[1] the technique was adapted to intrinsic stress measurements of thin metal films on silicon nitride membranes.[2] The method was extended to measure the Poisson's ratio of thin films utilizing rectangular samples with different aspect ratios.[3] Since then the bulge test has become a fairly well-characterized and widely accepted technique.[4,5]

Two major advantages associated with bulge test are the ease of specimen handling and the capability of imposing loading conditions. These advantages are unparalleled by other thin film testing methods such as nanoindentation, substrate-curvature technique, and microtensile testing. It is therefore not surprising that bulge test found many applications in the field of materials testing, where dynamic mechanical tests,[6–8] creep and viscoelastic tests,[9,10] and high-temperature testing[11] were reported. All these techniques require a more involved approach than that in a monotonic loading scenario, and bulge test is capable of providing a suitable platform in this regard. It is, of course, to be noted that even the case of monotonic loading is not straightforward and requires a considerable amount of attention for issues such as the displacement of the testing equipment under applied loads and the constancy of the applied strain rate.

The need for a constant strain rate is based on its effect on the strength measurement. It is well known that increasing the applied strain rate increases the flow stress of the specimen under testing. This effect becomes more pronounced at elevated temperatures. Strain rates utilized in mechanical testing cover a wide spectrum ranging from 10^{-8} s^{-1} (creep testing) to 10^{8} s^{-1} (hypervelocity impact testing).[12] The relation between flow stress σ and applied strain rate $\dot{\epsilon}$ at any given strain and temperature is described by the following relation:

$$\sigma = C(\dot{\epsilon})^m \quad , \tag{1}$$

where m is the strain-rate sensitivity. Although strain-rate sensitivity is usually low for metals at room temperature,[12] there is a general consensus that for Au thin films it increases with decreasing grain size.[13–16]

It is to be noted that although bulge test provides the capability for testing thin films under a constant strain-rate condition, reported use of it in a strain-rate-dependent material property measurement study is rare. Reports are usually limited to the testing of bulk materials such as niobium,[17] low-carbon steel,[18] and copper[19] sheets. An extensometer can be utilized together with a closed-loop servocontrol of the strain to increase the precision regarding the study of strain hardening.[20] This is

[a]Address all correspondence to this author.
e-mail: ealaca@ku.edu.tr
DOI: 10.1557/JMR.2008.0395

in contrast to thin films testing, where the measurement of strain has traditionally been a challenging task. Hence, imposing a constant strain rate does not constitute a straightforward task. A certain level of strain rate control for thin films is implemented through techniques including microscale tensile[13,15] or bending[16,21] tests with a constant cross-head and probe displacement rate, respectively. These techniques provide a nearly constant strain rate as the true-strain rate decreases with increasing strain if the cross-head velocity is kept constant. Therefore in the absence of a direct strain measurement technique such as the use of an extensometer, an open-loop approach is usually utilized where the cross-head displacement rate is adjusted according to the specimen length.[12] The imposed condition is maintained until the onset of non-uniformity of the plastic deformation.

In this work a similar approach was adopted for the bulge test. We demonstrate the use of a closed-loop bulge test for strain-controlled testing of submicron Au films, where a pronounced strain-rate dependency of the yield strength is observed. In the next section the condition for constant strain rate is discussed for high-aspect ratio, rectangular test samples. The description of the testing setup and sample preparation are followed by a discussion of the experimental procedure, where already established conditions are implemented as the control criterion. The paper is concluded by the validation of the proposed technique using test results obtained on 500-nm-thick, sputtered Au films, whose properties are fairly well documented in the literature.

II. CONDITION FOR CONSTANT STRAIN RATE

Specimens utilized in this work consist of rectangular membranes. The deflection h at the center of the membrane increases as a result of the applied pressure during the bulge test. The deflection is not only dependent on the applied pressure but it is also a function of the sample geometry and material parameters. In the elastic regime, for a linear elastic membrane, the relationship between the pressure P and the deflection h is given in a polynomial form[3,5] as

$$P = C_1 \frac{\sigma_0 d}{a^2} h + C_3 \frac{Ed}{(1-\nu)a^4} h^3 \quad , \tag{2}$$

where σ_0 is the in-plane biaxial residual stress, E is the elastic modulus, ν is the Poisson's ratio, d is the membrane thickness, and a is the half-width of the membrane. This model is a good approximation for membranes of different geometries. C_1 is a geometry dependent constant and C_3 depends on both the geometry of the membrane and the Poisson's ratio. For rectangular membranes with aspect ratios greater than 4, Eq. (2) can be further simplified to the following relation:

$$P = 2 \frac{\sigma_0 d}{a^2} h + \frac{4}{3} \frac{Ed}{(1-\nu^2)a^4} h^3 \quad . \tag{3}$$

In this case the stress state in the diaphragm can be approximated by the plane strain assumption. Equation (3) is used widely to extract residual stresses and elastic properties of thin films.

Stresses σ and strains ϵ in the specimen can also be calculated using the relations given in Eqs. (4) and (5) under the condition that the diaphragm width is much larger than the amount of deflections.

$$\sigma = \frac{Pa^2}{2hd} \quad , \tag{4}$$

$$\epsilon = \epsilon_0 + \frac{2h^2}{3a^2} \quad , \tag{5}$$

where ϵ_0 is the residual plane strain. Taking the first derivative of strain with respect to time t, the strain rate $\dot{\epsilon}$ can be derived as

$$\dot{\epsilon} = \frac{4}{3a^2} h \frac{\mathrm{d}h}{\mathrm{d}t} \quad . \tag{6}$$

Rearrangement of Eq. (6) as

$$\int_{h_0}^{h} \delta \mathrm{d}\delta = \int_{0}^{t} \dot{\epsilon} \frac{3a^2}{4} \mathrm{d}\tau \quad , \tag{7}$$

leads to the following expression:

$$h^2 = h_0^2 + \dot{\epsilon} \frac{3a^2}{2} t \quad . \tag{8}$$

For a flat membrane exposed to gauge pressure, the initial deflection h_0 is taken as zero. This is a condition that can easily be cross-checked prior to testing. Hence, the center displacement of a rectangular membrane at constant strain rate, $\dot{\epsilon}$ has a square-root time dependence as given below:

$$h = \frac{a\sqrt{6\dot{\epsilon}}}{2} t^{1/2} \quad . \tag{9}$$

Implementation of this condition in a bulge test setup is possible using a control algorithm. To evaluate h correctly, we utilize point measurements of displacements both at the center of the deforming diaphragm and the edge of the diaphragm where the substrate deflection is measured and eliminated from the readings. Compared to the interferometric method of measuring deflections, point measurement requires a considerable amount of alignment of the specimen with respect to the optical head. However, since obtained signals are from discrete and well-defined points, sensor output can be directly utilized in the control algorithm, and it becomes straightforward to impose the condition given in Eq. (9). In the

next section, details of the measurement will be discussed including experimental setup and sample preparation.

III. EXPERIMENTAL METHODS

A. Setup

Figure 1 provides a schematic illustration of the bulge test experiment. At the center of the setup lies the pressure chamber filled with hydraulic oil. It was machined out of steel and connected to a spring-loaded piston that is pushed by a piezoelectric actuator. The motion of the piston directly displaces hydraulic oil, and this displaced volume loads the specimen. The size of the piston is designed to optimize testing for diaphragm widths between 100 and 500 μm. The piezoelectric actuator provides a maximum travel of 100 μm (HVPZT-Translator by Physik Instrumente, Karlsruhe, Germany). The other end of the chamber provides a platform where the specimen is to be attached.

The setup provides two sets of data, i.e., the variable fluid pressure in the chamber and the accompanying center deflection of the membrane. There are two sensors serving these tasks.

(i) The pressure sensing device is a piezoresistive transmitter (Series PR-21S by Keller AG, Winterthur, Switzerland) generating an output in the range of 4-20 mA. After a conversion of the current output to voltage, a signal of 1 V corresponds to the atmospheric pressure while 5 V is the maximum limit indicating a pressure of 1 bar. The output range is scaled by 0.5% resolution. Pressure sensor is tightly screwed into the hydraulic oil chamber.

(ii) Specimen and substrate deflections are measured by a laser sensor (SLS 7000 by LMI Selcom, Partille, Sweden). The sensor works on the triangulation principle and measures the deflection of a single point. It is intended for operation on surfaces ranging from perfect mirrors to semi-specular surfaces. Therefore it is an ideal sensor for sputtered metallic thin films. A built-in camera enables the operator to place the laser spot of 10 μm diameter (GaAlAs, 675-nm wavelength) on the right location on the specimen. The stand-off distance is 15 mm. A change of 1 mA in the output signal corresponds to a 51.2-μm change in the absolute distance between the target and the sensor. The current output is then converted to voltage by a simple, home-built circuit. The obtained resolution is 0.25 μm.

Since deflection measurements are taken at specific points as opposed to mapping the deflection profile by an interferometric technique, the alignment of the specimen with respect to the laser sensor is important. Any misalignment will render obtained data useless as explained later in the discussion on the experimental procedure. Therefore the testing machine is placed on top of a six-degree-of-freedom stage with all possible rotational and translational movement capabilities embedded.

To attain sufficiently high pressures and accumulate enough deformation in the sample for plasticity, special attention is paid to purging trapped air from the system prior to testing. First of all, the amount of trapped air is minimized during sample mounting with the help of a paper sealant, which retains oil inside the central groove of the sample holder. The paper is removed once sample holder is pressed against the testing platform, where an O-ring prevents any leakage. It is rare that air is trapped in spite of this procedure. There is a window machined into the oil chamber to facilitate the observation of trapped air in the system. If any air is observed, the whole testing equipment can be rotated around its long axis, releasing the air pocket from underneath the sample into the main oil chamber. The chamber has a conical profile

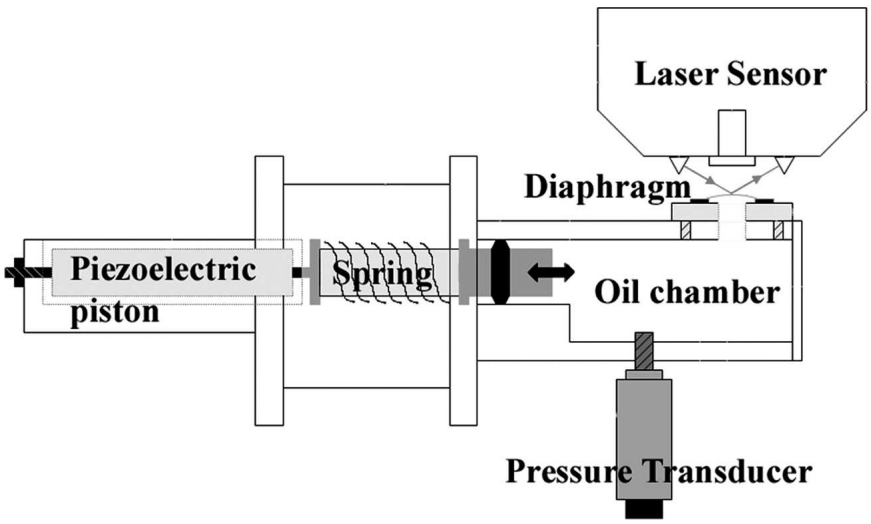

FIG. 1. Schematic illustration of the bulge test setup.

and a polished inner surface ensuring the collection of air bubbles at one of the ports, where a set of valves is used for purging purposes. Similarly, ports for the pressure sensor and purge valves are sealed against oil leakage. A channel gasket is used to seal the periphery of the reciprocating piston. As a result, a one-to-one correspondence between the piston motion and sample deflection is observed. Moreover, attained pressures could be kept constant over long periods of time. This was one of the most important aspects of experimental setup design for the success of the closed-loop control.

B. Sample preparation

Sample preparation requires a two-mask, double-sided lithography process. The first lithography step is used to define Ti cross-hair structures indicating the midpoint of each Au diaphragm. The second lithography process defines the etch mask on the other side of the wafer, where the substrate material is to be etched for releasing the diaphragms.

The fabrication sequence is summarized in Fig. 2. A 4-in.-diameter ⟨111⟩ Si wafer with a thickness of 200 ± 10 μm and a resistivity of 5 mΩ cm was used as the substrate. The wafer first underwent Piranha cleaning and buffered oxide etch (BOE). At the end of each process, the wafer was rinsed with de-ionized (DI) water (5 cycles after Piranha cleaning and 3 cycles after BOE) and dry-blown with N_2. Finally, cleaned wafer was baked in N_2 at 110 °C for 15 min for dehydration where it became ready for metal deposition.

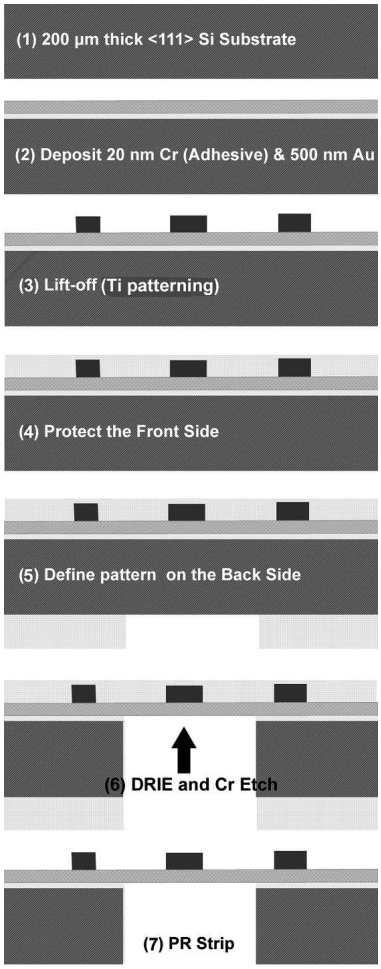

FIG. 2. Fabrication sequence.

Layers of 20-nm Cr and 500-nm Au were sputtered onto the Si wafer. The first photolithography was applied on the Au layer, which is referred as the front side of the wafer. Prior to the deposition of the photoresist (S1828), hexamethyldisilazane (HMDS) was applied on the Au surface as an adhesion promoter. Then, photoresist (PR) was soft-baked for 1 min at 115 °C followed by ultraviolet (UV) exposure and development. The wafer was rinsed with DI water twice, (first for 2.5 min and then for 1 min) and dried with N_2. O_2 plasma was then applied for 3 min to ensure that there was no excessive PR leftover followed by a hard-bake at 115 °C for 30 min. A 10-nm-thick Ti layer was sputtered followed by a lift-off in acetone. Ti cross-hair structures indicating the midpoint of each diaphragm were thus defined. A dehydration step was carried out at 110 °C in N_2 for 20 min. Au surface with Ti cross-hairs was covered with a protective PR layer and baked at 115 °C for 30 min.

The second photolithography took place on the back side of the wafer. A procedure similar to the first lithography was followed. After the application of HMDS, PR (SPR220-7) was spin-coated. After soft-bake for 30 min, alignment, exposure and development took place. DI rinse, N_2 dry, and O_2 plasma were carried out. After a hard-bake at 115 °C for 30 min, deep reactive-ion etching (DRIE) was utilized to anisotropically etch Si substrate and release the diaphragm structures. The Cr layer was removed by wet etching.

PR layers on both sides of the wafer were stripped (SVC-175). The metal side was covered with a new protective PR layer. The wafer was finally diced into square test chips. The chips were directly attached to the sample holder of the testing setup.

C. Testing procedure

After fabrication, the diced chips were stored in a Petri dish. Before testing, each chip was rinsed with acetone to remove the protective PR layer on the Au surface. The chip was then rinsed with isopropyl alcohol and DI water. Each cleaned chip was attached on the center of a sample holder using epoxy. The sample holder was a thin Al plate with a hole in the middle through which hydraulic oil could exert pressure on the diaphragms. After curing of epoxy, the plate was screwed to the testing platform on the pressure chamber, and an O-ring ensured sealing between the sample holder and the pressure

chamber. During clamping, the pressure had to be monitored continuously to prevent excessive loading of the diaphragms. Opening purge valves during this step prevented build-up of pressure. Finally the chamber was inspected for trapped air.

The next step in the testing procedure was the alignment of the specimen with respect to the laser sensor. As mentioned before, alignment was crucial for obtaining reliable data. Figure 3 explains the major steps. Assume that the plane of the specimen is defined by x and y axes. The z axis is normal to this plane. The coordinates associated with the diaphragm are given by ξ and η. ξ defines the long axis of the diaphragm and η defines the direction along which the maxima of the bulging shape move as a result of the increased pressure. Finally, plane π is spanned by the incoming and reflected laser beams. The alignment procedure consists of two steps. First, the out-of-plane alignment is to be carried out [Fig. 3(a)]. By rotating the sample around x and y axes and scanning the sample with the laser spot, one can ensure that every point on the specimen is equally distant from the sensor head. In-plane alignment is the next step, where the specimen is rotated around the z axis, until ξ coincides with the π plane. This ensures that the bulging shape of the diaphragm will not obstruct the incoming beam irrespective of how much the specimen is inflated. The maxima at different pressures, A, B, and C, will be confined to the π plane, and therefore the diaphragm will act as a perfectly horizontal plane moving towards the sensor head. Under any other condition, the triangulation measurement principle of the sensor would yield erroneous data. At this point, it should also be mentioned that the size of the focused beam (10 μm) is negligible compared to the arc length of the bulging diaphragms used in this study. Hence, measurements can be considered to be taken at a single point.

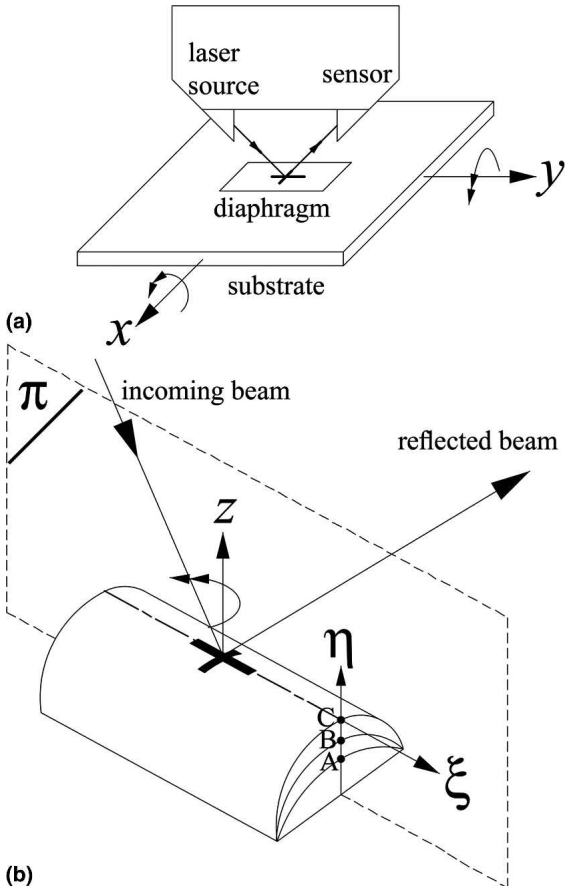

FIG. 3. Alignment of the specimen with respect to the displacement sensor. (a) Out-of-plane alignment is carried out by utilizing rotation around x and y axes. As a result of this procedure, all points on the specimen become equally distant from the sensor head. (b) Close-up of the bulging diaphragm. In-plane alignment is carried out by rotating the sample around the z axis such that the long axis of the diaphragm, designated by ξ, coincides with the plane π. Hence, the bulging diaphragm acts as a perfectly horizontal plane moving toward the sensor head. This eliminates the disadvantage of point measurement associated with the triangulation principle.

Once the alignment step was accomplished, the laser probe was moved to the center of the diaphragm, which is indicated by a 10-nm-thick, 10-μm-wide Ti cross-hair, shown in Fig. 3. The loading was initiated with the closed-loop criterion imposed by an automation program (Labview by National Instruments, Austin, TX). The criterion had to be, of course, modified to accommodate the effect of the substrate deflection. In this study, a 200-μm-thick Si wafer was used as the substrate. Such thickness was necessary to minimize the duration of the DRIE process. However, it also led to a decreased stiffness of the substrate to an extent that its deflection h_s under the applied pressure could not be neglected [Fig. 4(a)].

To show the effect of substrate deflection, a typical loading experiment was performed in which the displacement data h_s were taken from a point on the substrate close to the edge of the diaphragm. The typical effect of the substrate deflection can be observed in Fig. 5 for a 320-μm-wide diaphragm, where the pressure versus deflection behavior of the diaphragm is different from that when h_s is not eliminated.

Since this type of measurement does not overrule the possibility of the delamination of the Au diaphragm from its substrate, another experiment was necessary, where a sample was prepared upside down and a final measurement was taken on the backside, where bare Si was exposed [Figs. 4(b) and 4(c)]. Under these conditions, a similar deflection behavior was observed linking displacement measurements at the edge of the sample directly to the deflection of the substrate.

Removing the substrate deflection h_s from the total displacement of the diaphragm, h_t was necessary to obtain net deflection h in Eq. (9). Both experiments and finite element simulations showed a linear relationship between h_s and the applied pressure P.

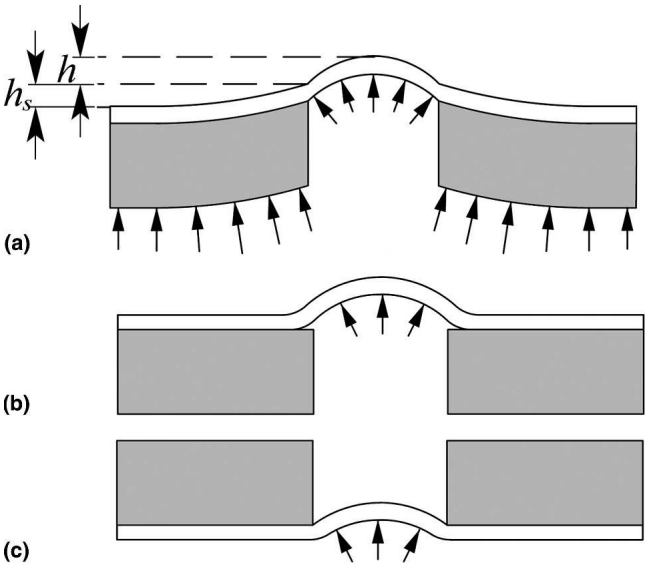

FIG. 4. (a) Total deflection at the center of the diaphragm is the sum of the substrate deflection and the actual deflection of the diaphragm. (b) Higher deflection reading can also result from a delamination of the thin film from the substrate. (c) The effect of delamination can be evaluated by testing the sample upside down.

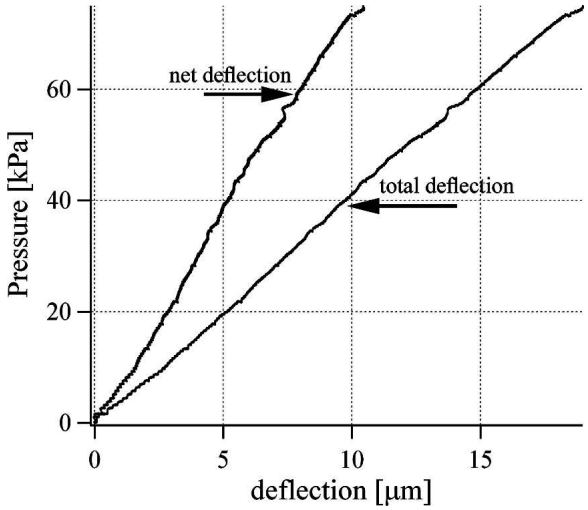

FIG. 5. Pressure versus deflection graph of a 320-μm-wide diaphragm showing the effect of substrate deflection.

$$P = \alpha h_s \quad . \tag{10}$$

The proportionality constant α can be retrieved from a linear fit of the pressure versus deflection data. α was unique for each set of dice with a certain number of diaphragms and diaphragm dimensions. Therefore proportionality constant had to be determined for each set of specimens experimentally.

After some manipulation of Eq. (9), one arrives at the following relation in terms of total measured deflection h_t.

$$h_t = \frac{2\sigma_0 d + \alpha a^2}{2\alpha a}\sqrt{6\dot{\epsilon}}\, t^{1/2} + \frac{Ed}{(1-\nu^2)\alpha a}\sqrt{6\dot{\epsilon}^3}\, t^{3/2} \quad . \tag{11}$$

This relation was implemented to the main Labview routine. For each test, temporal evolution of strain was plotted to check the validity of the control criterion. An example is given in Fig. 6 for two separate tests with imposed strain rates of 2.0×10^{-4} and 3.0×10^{-5} s^{-1}. For the test where a strain rate of 2.0×10^{-4} s^{-1} was imposed, analysis of experimental data yielded an average strain rate of 1.7×10^{-4} s^{-1} with a standard deviation of 6×10^{-5} s^{-1}. For the 3.0×10^{-5} s^{-1} test, the average strain rate was calculated to be 3.0×10^{-5} s^{-1} with a standard deviation of 1.7×10^{-5} s^{-1}. The deviation from linearity for the slow test beyond 30 s is noteworthy. For the faster test, the deviation occurs earlier. However, yielding in both cases was observed within the linear regime justifying the reliability of the yield strength measurement.

In the next section, the validation of the technique is carried out by comparing results obtained from Au samples with those reported in the literature.

IV. VALIDATION

First of all, to justify the use of the spot measurement technique accompanied by the elimination of the substrate deflection, elastic measurements are compared

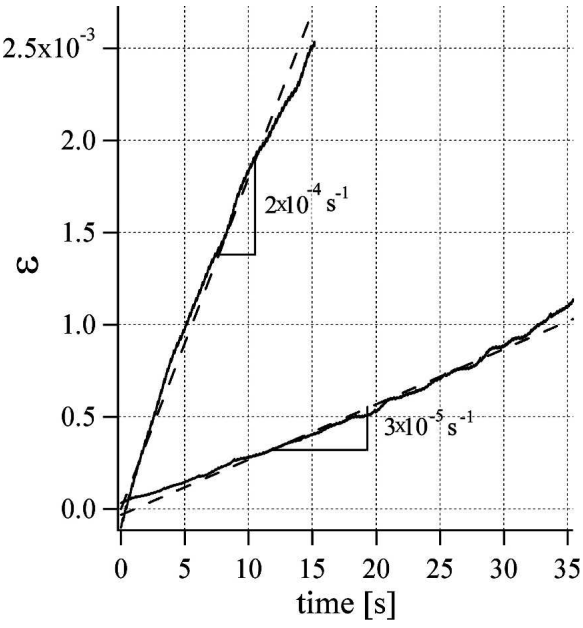

FIG. 6. Strain versus time graph for a 320-μm-wide diaphragm. The slope of the linear fit line (dashed) corresponds to the applied strain rate. The deviation of the applied strain from linearity toward the end of the test is noteworthy. However, specimens yielded much earlier, ensuring that the yield strength data were obtained at a constant strain rate. Yield points can be observed in Fig. 7.

with those reported in the literature. The elastic modulus E and the residual stress σ_0 of the 500-nm-thick Au specimens of this study were extracted from Eq. (3) as 51.1 ± 12.2 GPa and 134.8 ± 35.2 MPa, respectively, for a Poisson's ratio of 0.425.[22] These findings were observed to be independent of the applied strain rates. An extreme ⟨111⟩ texture was evident from x-ray diffraction measurements as expected.[14,16] The grain size was also found to be below 100 nm.

In the literature, similar modulus values are reported for Au films.[14,16,21,23,24] Furthermore, a specific study with a similar grain size and texture revealed no dependence of the elastic modulus on the applied strain rate.[16] This is in contradiction to reports on Au films with slightly bigger grain sizes.[14,15] It should also be noted that the measured value for the modulus is still far from that computed using the compliance tensor obtained from x-ray diffraction data.[22] As is the case for any other thin film material, the cause of such variation in modulus can be traced back to the common complication arising from the use of different measurement and/or growth techniques.[4]

Yield strength measurements were carried out by imposing strain rates that ranged from 2×10^{-6} to 2×10^{-4} s^{-1}. Strain range used was on the order of 10^{-3}, enough to initiate yielding. Two examples of obtained stress–strain graphs are shown in Fig. 7. In these plots, one order of magnitude difference in the applied strain rate is observed to lead to an appreciable difference in yield strengths. It should be emphasized that for each test, a linear temporal evolution of strain was verified as discussed previously in relation to Fig. 6.

The resulting variation of yield strength as a function of applied strain rate is given in Fig. 8 over the complete

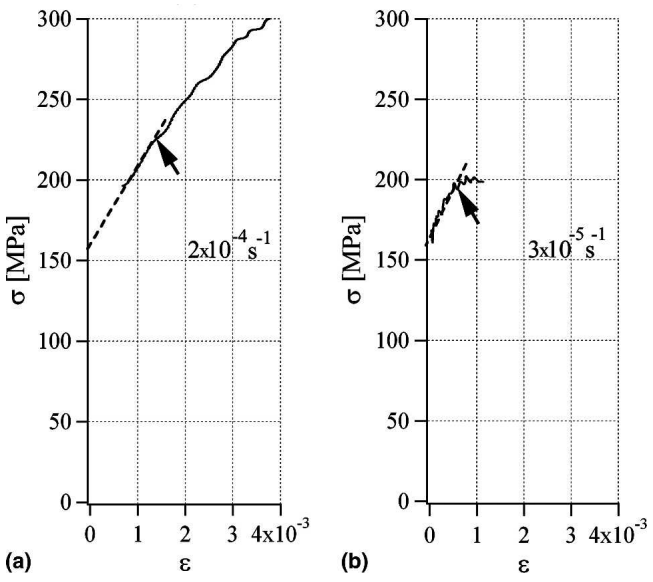

FIG. 7. Stress–strain graphs at different strain rates.

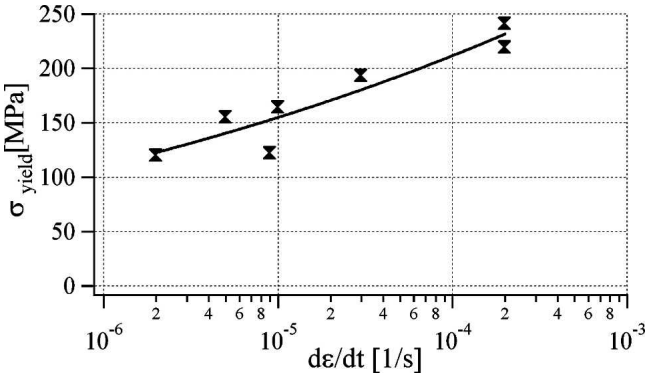

FIG. 8. Variation of the plane-strain yield strength with the applied strain rate.

strain-rate spectrum along with a power fit. The total sum of the squared errors is estimated to be 1651 MPa^2. Strain-rate sensitivity m, given in Eq. (1) is calculated as 0.11 from this plot. This value is similar to 1/9.3 which was recently measured by Wang and Prorok[16] for 500-nm-thick Au films with a similar texture and grain size distribution. However, their strength measurements are consistently 1.5 times higher than those reported in Fig. 8. The actual deviation will be larger because of the fact that stresses in Fig. 8 are plane-strain values, and hence they are expected to slightly exceed uniaxial stresses required for yielding.

V. CONCLUSIONS

The approach of this work to apply a constant strain rate during deformation is similar to that utilized in the uniaxial testing, where the following temporal evolution of the deformation velocity v is imposed on a sample of length l_0[12]

$$v = \dot{\epsilon} l_0 \exp(\dot{\epsilon} t) \quad , \tag{12}$$

with the exception that a closed-loop control is necessary in bulge test. This imposed condition leads to a constant strain rate until the onset of nonuniformity. Direct measurement of strain via an extensometer or a similar tool would enhance the control. However, for thin film testing, this poses a considerable challenge. Nearly constant strain rates in the literature on thin films are therefore obtained by applying a constant cross-head displacement in microtensile testing[14,15] or a constant probe displacement in microbending testing.[16,21] Due to the same difficulty, the widely accepted plane-strain formulation for bulge test can be utilized to convert measured displacements into strains.

The spot measurement of displacements was observed to raise the need for the consideration of (1) the alignment of the specimen with respect to the optical measurement device, and (2) a separate measurement of the substrate deflection. The first issue was dealt with using

a six-degree-of-freedom stage allowing high precision in the alignment of the specimen. The alignment of the long-axis of the diaphragm with respect to the plane of the laser beam was also of importance in this regard. The second issue was addressed by careful measurements of substrate deflection and embedding of the effect in the closed-loop criterion. In spite of these associated difficulties, the spot measurement was still advantageous in obtaining a single analog signal that could directly be used in the control algorithm without the need for further signal processing.

ACKNOWLEDGMENTS

This work was supported by Koc University (KU). B.E.A. wishes to thank N. Veryeri, M.Sci., of Veryeri Makina for designing the testing apparatus. Help from A. Yetistiren and I. Veryeri of KU and O. Gurkan of Ziya Atolyesi for building the apparatus is acknowledged. X-ray diffraction work was carried out by Prof. H. Maier of Paderborn University. Prof. D. Canadinc of KU is thanked for discussions regarding microstructural aspects.

REFERENCES

1. J.W. Beams: Mechanical properties of thin films of gold and silver, in *Proceedings of International Conference on Structure and Properties of Thin Films*, edited by C.A. Neugebauer, J.B. Newkirk, and D.A. Vermilya (John Wiley, NY, 1959), pp. 183–192.
2. E.I. Bromley: A technique for the determination of stress in thin films. *J. Vac. Sci. Technol., B* **1,** 1364 (1983).
3. J.J. Vlassak and W.D. Nix: A new bulge test technique for the determination of Young's modulus and Poisson's ratio of thin films. *J. Mater. Res.* **7,** 3242 (1992).
4. R.L. Edwards, G. Coles, and W.N. Sharpe, Jr.: Comparison of tensile and bulge tests for thin-film silicon nitride. *Exp. Mech.* **44,** 49 (2004).
5. Y. Xiang, X. Chen, and J.J. Vlassak: Plane-strain bulge test for thin films. *J. Mater. Res.* **20,** 2360 (2005).
6. A.J. Kalkman, A.H. Verbruggen, and G.C.A.M. Janssen: Young's modulus measurements and grain boundary sliding in free-standing thin metal films. *Appl. Phys. Lett.* **78,** 2673 (2001).
7. J.D. Hall, N.E. Apperson, B.T. Crozier, C. Xu, R.F. Richards, D.F. Bahr, and C.D. Richards: A facility for characterizing the dynamic mechanical behavior of thin membranes for microelectromechanical systems. *Rev. Sci. Instrum.* **73,** 2067 (2002).
8. B.E. Alaca, J.C. Selby, M.T.A. Saif, and H. Sehitoglu: Biaxial testing of nanoscale films on compliant substrates: Fatigue and fracture. *Rev. Sci. Instrum.* **73**(8), 2963 (2002).
9. A.J. Kalkman, A.H. Verbruggen, G.C.A.M. Janssen, and S. Radelaar: Transient creep in free-standing thin polycrystalline aluminum films. *J. Appl. Phys.* **92,** 4968 (2002).
10. S. Hyun, T.K. Hooghan, W.L. Brown, and R.P. Vinci: Linear viscoelasticity in aluminum films. *Appl. Phys. Lett.* **87,** 061902 (2005).
11. M. Cieslar, V. Oliva, A. Karimi, and J-L. Martin: Plasticity of thin Al films as a function of temperature. *Mater. Sci. Eng., A* **387–389,** 734 (2004).
12. G.E. Dieter: *Mechanical Metallurgy*, SI Metric ed. (McGraw-Hill Book Company, Singapore, 1988), pp. 295–301.
13. R.D. Emery and G.L. Povirk: Tensile behavior of free-standing gold films. Part I. Coarse-grained films. *Acta Mater.* **51,** 2067 (2003).
14. R.D. Emery and G.L. Povirk: Tensile behavior of free-standing gold films. Part II. Fine-grained films. *Acta Mater.* **51,** 2079 (2003).
15. I. Chasiotis, C. Bateson, K. Timpano, A.S. McCarty, N.S. Barker, and J.R. Stanec: Strain rate effects on the mechanical behavior of nanocrystalline Au films. *Thin Solid Films* **515,** 3183 (2007).
16. L. Wang and B.C. Prorok: Characterization of the strain rate dependent behavior of nanocrystalline gold films. *J. Mater. Res.* **23,** 55 (2008).
17. A. Zamiri, F. Porboghrat, H. Jiang, T.R. Bieler, F. Barlat, J. Brem, C. Compton, and T.L. Grimm: On mechanical properties of the superconducting niobium. *Mater. Sci. Eng., A* **435–436,** 658 (2006).
18. P. Broomhead and R.J. Grieve: The effect of strain rate on the strain to fracture of a sheet steel under biaxial tensile stress conditions. *J. Eng. Mater. Technol. Trans. ASME* **104,** 102 (1982).
19. G. Montay, M. François, M. Tourneix, B. Guelorget, C. Vial-Edwards, and I. Lira: Strain and strain-rate measurement during the bulge test by electronic speckle pattern interferometry. *J. Mater. Process. Technol.* **184,** 428 (2007).
20. M. Atkinson: An investigation of hydraulic bulging as a biaxial straining test for sheet metal. *J. Test. Eval.* **33,** 537 (2005).
21. H.D. Espinosa, B.C. Prorok, and B. Peng: Plasticity size effects in free-standing submicron polycrystalline FCC films subjected to pure tension. *J. Mech. Phys. Solids* **52,** 667 (2004).
22. P-O. Renault, E. Le Bourhis, P. Villain, Ph. Goudeau, K.F. Badawi, and D. Faurie: Measurement of the elastic constants of textured anisotropic thin films from x-ray diffraction data. *Appl. Phys. Lett.* **83,** 473 (2003).
23. R.P. Vinci and J.J. Vlassak: Mechanical behavior of thin films. *Annu. Rev. Mater. Sci.* **26,** 431 (1996).
24. W.D. Nix: Mechanical properties of thin films. *Metall. Trans. A* **20,** 2217 (1989).